TDP-43 transgenic mice develop spastic paralysis and neuronal inclusions characteristic of ALS and frontotemporal lobar degeneration

Hans Wils[a,b,c], Gernot Kleinberger[a,b,c], Jonathan Janssens[a,b,c], Sandra Pereson[a,b,c], Geert Joris[a,b,c], Ivy Cuijt[a,b,c], Veerle Smits[a,b,c], Chantal Ceuterick-de Groote[c,d], Christine Van Broeckhoven[a,b,c], and Samir Kumar-Singh[a,b,c,1]

[a]Neurodegenerative Brain Diseases Group, Department of Molecular Genetics, VIB, B-2610 Antwerpen, Belgium; [b]Laboratory of Neurogenetics and [d]Laboratory of Ultrastructural Neuropathology, Institute Born-Bunge, B-2610 Antwerpen, Belgium; and [c]University of Antwerp (CDE), B-2610 Antwerpen, Belgium

Edited by Stanley Appel, Methodist Research Institute, and accepted by the Editorial Board January 6, 2010 (received for review October 27, 2009)

Neuronal cytoplasmic and intranuclear aggregates of RNA-binding protein TDP-43 are a hallmark feature of neurodegenerative diseases such as amyotrophic lateral sclerosis (ALS) and frontotemporal lobar degeneration (FTLD). ALS and FTLD show a considerable clinical and pathological overlap and occur as both familial and sporadic forms. Though missense mutations in TDP-43 cause rare forms of familial ALS, it is not yet known whether this is due to loss of TDP-43 function or gain of aberrant function. Moreover, the role of wild-type (WT) TDP-43, associated with the majority of familial and sporadic ALS/FTLD patients, is also currently unknown. Generating homozygous and hemizygous WT human TDP-43 transgenic mouse lines, we show here a dose-dependent degeneration of cortical and spinal motor neurons and development of spastic quadriplegia reminiscent of ALS. A dose-dependent degeneration of nonmotor cortical and subcortical neurons characteristic of FTLD was also observed. Neurons in the affected spinal cord and brain regions showed accumulation of TDP-43 nuclear and cytoplasmic aggregates that were both ubiquitinated and phosphorylated as observed in ALS/FTLD patients. Moreover, the characteristic ≈25-kDa C-terminal fragments (CTFs) were also recovered from nuclear fractions and correlated with disease development and progression in WT TDP-43 mice. These findings suggest that ≈25-kDa TDP-43 CTFs are noxious to neurons by a gain of aberrant nuclear function.

protein aggregation | neurodegeneration | dementia | motor neuron disease | FTLD

Amyotrophic lateral sclerosis (ALS) is one of the most common progressive neuromuscular diseases worldwide and is characterized by degeneration of cortical motor neurons, the motor nuclei of the brainstem, and the anterior horn cells of the spinal cord. Dysfunction and death of these neurons lead to muscle weakness, atrophy, and spasticity (1). Frontotemporal lobar degeneration (FTLD) is the second most common form of cortical dementia in the presenium, accounting for ≈20% of dementia patients in this age group (2). Both ALS and FTLD patients are characterized by ubiquitinated neuronal cytoplasmic and intranuclear inclusions (NCIs and NIIs) in affected brain regions (2). Approximately 20% of patients with ALS show frontal lobe dysfunction that overlaps with the pathology of FTLD, suggesting that FTLD and ALS are part of the same disease spectrum (3).

The recent identification of the TAR DNA-binding protein-43 (TDP-43) as a major protein constituent of NCIs and NIIs in ALS and FTLD (FTLD-U or FTLD-TDP) patients has offered a molecular link between these two disorders (4, 5). TDP-43 is a 414-amino acid protein with two highly conserved RNA recognition motifs (RRM1 and RRM2), a nuclear localization signal (NLS) at the protein N-terminus, and a glycine-rich region mediating protein–protein interactions at the C-terminus (6–9). Pathological TDP-43 is abnormally ubiquitinated, hyperphosphorylated, and N-terminally cleaved to generate CTFs (4, 5).

Missense mutations in the TDP-43 gene (*TARDBP*), mostly in the C-terminal glycine-rich region, have been identified in patients with ALS (10, 11), and ALS associated with FTLD (12). However, in FTLD and in the majority of familial and sporadic ALS patients, no *TARDBP* mutations are identified, suggesting that wild-type (WT) TDP-43 is central to the disease cascade (9, 13). Recently, overexpression of the TDP-43 homolog in yeast or injections of viral hTDP-43 constructs in the substantia nigra of rats have been shown to cause cell death (14, 15). To identify neurons specifically vulnerable to increased TDP-43 levels, we generated germline transgenic mouse lines overexpressing human *TARDBP* ($TDP43^{WT}$). We show here that overexpression of WT TDP-43 leads to degeneration of specific neurons in the central nervous system, including spinal and cortical motor neurons and nonmotor cortical neurons characteristically affected in FTLD-TDP, and causes spastic quadriplegia in a dose-dependent manner.

Results

Dose-Dependent Motor Neuron Disease in $TDP43^{WT}$ Mice. We generated several germline transgenic mouse lines overexpressing human wild-type *TARDBP* ($TDP43^{WT}$) under the control of a neuronal murine Thy-1 (mThy-1) promoter that drives transgene expression in virtually all neurons of the central nervous system (Fig. 1*A*) and becomes active approximately 1 week after birth (16). Transgene levels in total brain lysates were analyzed by semiquantitative real-time PCR (Q-RT-PCR) (Fig. 1*B*) and immunoblotting with anti-TDP-43 antibodies (Fig. S1). In none of the $TDP43^{WT}$ lines did TDP-43 expression exceed 1× endogenous TDP-43 expression. To increase transgene dose, we generated homozygous mice from the two highest-expressing founder lines. Homozygous TAR4/4 and TAR6/6 lines showed a double transgene expression (2× and 1.2×, respectively) compared with hemizygous TAR4 and TAR6 lines with 1× and 0.6× hTDP-43 levels over endogenous protein levels (Fig. 1*B* and Fig. S1). Because Thy-1 expression is limited to neurons, we also analyzed hTDP-43 expression relative to murine TDP-43 by Q-RT-PCR in neurons isolated from 1-month-old $TDP43^{WT}$ mice (17), and also by immunohistochemical densitometric quantification (18) (Fig. S1). On ≈5-fold-enriched neuronal preparations, TAR4 and TAR6 mice showed 1.4-fold and 0.9-fold

Author contributions: H.W., C.V.B., and S.K.-S. designed research; H.W., G.K., J.J., S.P., G.J., I.C., V.S., and S.K.-S. performed research; C.C.-d.G. contributed new reagents/analytic tools; H.W., G.K., J.J., S.P., and S.K.-S. analyzed data; and H.W., C.V.B and S.K.-S. wrote the paper.

The authors declare no conflict of interest.

Freely available online through the PNAS open access option.

This article is a PNAS Direct Submission. S.A. is a guest editor invited by the Editorial Board.

[1]To whom correspondence should be addressed. E-mail: samir.kumarsingh@ua.ac.be.

This article contains supporting information online at www.pnas.org/cgi/content/full/0912417107/DCSupplemental.

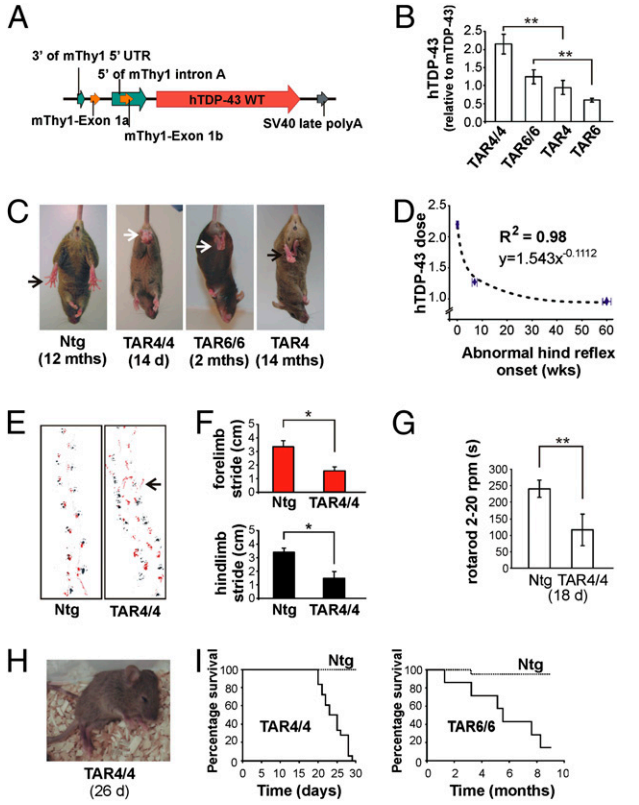

Fig. 1. hTDP-43 overexpression in mice leads to a dose-dependent motor neuron disease phenotype. (*A*) Schematic drawing of the Thy-1 expression vector used to generate transgenic TDP43^{WT} lines. (*B*) mRNA expression levels in brain measured by Q-RT-PCR for different transgenic lines (**$P <$ 0.01). (*C*) Abnormal limb reflex in TDP43^{WT} lines at different ages. (*D*) A log-log correlation of hTDP-43 dosage in TAR4/4, TAR6/6, and TAR4 mice with the age at which the abnormal limb reflex was first noticed. (*E*) Disturbed footprint pattern in TAR4/4 mice with markedly wide-based stance, small stride, and frequent off-line stumbling in transgenic mice (arrow). (*F*) Significant 2-fold decrease in the stride of both forelimb (red) and hindlimb (black) (*$P < 0.05$). Data are presented as mean ± SD (*G*) Approximately 2.5-fold reduced performance of TAR4/4 mice on accelerating rotarod compared with Ntg littermates (**$P < 0.01$). (*H*) End-stage paralysis in TAR4/4 mice (Movie S1). (*I*) Survival curve of TAR 4/4 mice showed an average survival of 24 days, and 6.7 months for TAR6/6 mice.

hTDP-43 over murine TDP-43. Image densitometry of neuronal TDP-43 staining by a non-species-specific TDP-43 antibody further confirmed that TAR4 and TAR6 had 2.8- and 1.9-fold, and homozygous TAR4/4 and TAR6/6 had 5.1- and 3.8-fold hTDP-43 expression, compared with murine TDP-43 in non-transgenic (Ntg) mice (Fig. S1).

Homozygous TDP43^{WT} mouse lines were morphologically indistinguishable from their hemizygous or Ntg littermates at birth. At ≈14 days, TAR4/4 mice developed an abnormal hindlimb reflex characterized by retraction of hindlegs toward the trunk upon lifting them by their tail, as opposed to Ntg littermates, which showed normal extension of the legs (Fig. 1*C*). This reflex was demonstrated as one of the earliest symptoms of loss of motor control in several ALS mouse models (19). A footprint analysis for TAR4/4 mice showed a significant ≈2-fold decrease in the stride of hindlimbs (1.5 ± 0.26 cm vs. 3.4 ± 0.32 cm; $P = 0.025$) and of forelimbs (1.5 ± 0.19 cm vs. 3.3 ± 0.41 cm; $P <$ 0.01). Moreover, footprints of TAR4/4 mice were characterized by separated forelimb and hindlimb prints, markedly wide-based stance, small stride, and frequent off-line stumbling compared with Ntg littermates, which showed a normal, narrow-based stance with steady, close-proximity forelimb and hindlimb footprints (Fig. 1 *E* and *F*). When tested for motor performance on accelerating rotarod, 18-day-old TAR4/4 mice showed a statistically significant ≈2.5-fold reduced performance compared with Ntg littermates (114.2 ± 51.10 s vs. 236.2 ± 31.47 s; $P <$ 0.01) (Fig. 1*G*). At ≈22 days, fasciculations and spasms of facial muscles were also observed, which was followed by an extremely rapid disease progression, with mice becoming completely paralyzed and dying within 3–4 days (Fig. 1 *H* and *I* and Movie S1).

To verify that the hTDP-43 construct did not cause insertional mutagenesis of a mouse endogenous gene leading to the observed phenotype, we characterized the transgene integration site in the TAR4 mouse line. A thermal asymmetric interlaced PCR analysis showed that hTDP-43 had integrated at locus 6qB3 of the mouse genome (nucleotide no. 56,524,796; UCSC Genome Browser, http://www.genome.ucsc.edu/) and did not interrupt any known gene.

Subsequently, motor problems also developed in TAR6/6 and TAR4 mice (Table S1). TAR6/6 mice developed abnormal limb reflex at 2 months, showed up to 6-fold reduced motor performance at ≈4 months ($P < 0.01$; Fig. S2), and an average survival of 6.7 months (Fig. 1*I*). Similarly, TAR4 mice showed abnormal limb reflex at ≈14 months and 40% reduced motor performance at ≈15 months of age ($P < 0.01$; Fig. S2). Thus, correlation of hTDP-43 expression in TAR4/4, TAR6/6, and TAR4 mice with age of disease onset was best explained by a log-log regression model (correlation coefficient $R^2 = 0.98$; $P < 0.001$; Fig. 1*D*). No clinical phenotype has been observed in the TAR6 hemizygous mice analyzed until 19 months or in any other founder lines analyzed until 7 months, all expressing hTDP-43 ≤ 0.6× the endogenous TDP-43 level on total brain lysates. Thus, TDP43^{WT} mice have a dose-dependent ALS-like phenotype, influencing both onset and progression of the disease.

TDP43^{WT} Mice Display Neuropathology Reminiscent of FTLD/ALS. One of the chief pathological findings in ALS and FTLD-TDP brains are neuronal nuclear and cytoplasmic inclusions composed of ubiquitinated and phosphorylated TDP-43 (4, 5, 20). We therefore first examined brains of TAR4/4, TAR6/6, and TAR4 mice by ubiquitin immunohistochemistry. Despite mThy-1 promoter driving transgene expression in virtually all neurons of the brain, dense, large NCIs and NIIs characteristic of FTLD and ALS patients were present solely in cortical layer V of the anterior cortex, including primary motor cortex and somatosensory areas of the hind- and forelimbs, and also to some extent in hippocampal/subicular neurons (Fig. 2 *A*–*C* and Fig. S3). A dose-dependent, diffuse ubiquitin immunostaining was also present in brainstem, cranial motor nuclei, and Purkinje cells, but was absent from other brain regions, including neostriatum, substantia nigra, and thalamus. Using a panel of TDP-43-specific antibodies, including phosphospecific TDP-43 antibodies (21), we further showed that though NIIs always costained for TDP-43, a proportion of NCIs did not stain with TDP-43 antibodies (Fig. 2 *B* and *C*). The presence of NCIs, and to some extent NIIs, also coincided with an overall decreased nuclear TDP-43 reactivity, or "clearing," as described for ALS and FTLD patients (4, 5).

Interestingly, dose-dependent astrogliosis and microgliosis were also observed in TAR4/4, TAR6/6, and TAR4 mice in the same regions where NCIs, NIIs, and diffuse cytoplasmic ubiquitin staining was observed (Fig. S4). For TAR4/4, glial fibrillary acidic protein (GFAP) selectively stained cortical layer V of the anterior cortex, including the motor and somatosensory cortex (Fig. 2*D*). Neuronal loss was also present in affected brain regions of all mouse lines in both superficial and deep cortical layers of the anterior cortex, especially in higher-expressing TAR4/4 and TAR6/6 mice. Quantitative neuronal loss was shown in motor cortex of TAR4/4 mice compared with Ntg littermates at 24 days (867 per mm^2 ± 195 vs. 1,231 ± 181; $P <$

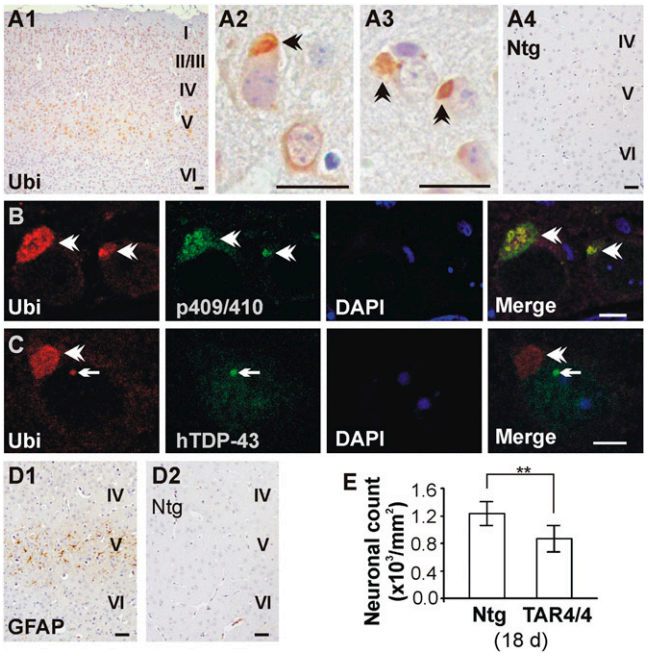

Fig. 2. NCI and NII brain pathology in TDP43^{WT} mice. (*A*) Ubiquitin pathology in layer V of the motor and somatosensory cortex of TAR4/4 but not in Ntg mice. *A2* and *A3* are higher magnifications. (Scale bars: 20 μm.) (*B* and *C*) Colabeling of ubiquitin-positive aggregates with p409/410 and human-specific TDP-43 antibodies showing NCIs (*B*, arrowheads) and NIIs (*C*, arrows). (Scale bars: 5 μm.) (*D*) Increased GFAP staining in cortical layer V of motor cortex that is absent in Ntg mice. (Scale bars: 20 μm.) (*E*) Quantification of the neuronal loss showed ≈30% reduction in cortical layer V of TAR4/4 mice compared with Ntg littermates (**$P < 0.01$).

0.001) and of TAR6/6 mice at 6 months (969 ± 187 per mm^2 vs. 1,149 ± 185; $P < 0.01$; Fig. 2*E* and Fig. S3). Vacuolar degeneration of several cranial motor nuclei was also observed, especially for the highest-expressing TAR4/4 line. In addition, TAR4/4 mice showed loss of CA3 hippocampal neurons and degeneration of Purkinje cells. These data are consistent with mutant superoxide dismutase 1 (SOD1) mice, where in low doses, the spinal cord is primarily affected, and in higher doses, other regions are also affected (22, 23). Moreover, a preferentially higher expression of hTDP-43 is shown to occur in the hippocampus (24), and degeneration of susceptible hippocampal cellular population is commonly observed in FTLD-TDP patients (25). Cerebellum is also shown to be severely affected in ALS patients (26). Thus, TDP43^{WT} mice recapitulate FTLD/ALS pathology, including the characteristic NCIs and NIIs. Interestingly, these pathological changes were accompanied by increased levels of activated caspase-3 and cleaved poly(ADP-ribose) polymerase (PARP) (Fig. S5), additionally suggesting that neuronal apoptosis is a hallmark of TDP-43 proteinopathies.

Because TAR4/4, TAR6/6, and TAR4 mice also showed an ALS phenotype, we next focused our attention on the spinal cord of these TDP43^{WT} mice (Fig. 3 and Fig. S3). Atrophy and increased number of pyknotic neurons in the ventral horn region of the lumbosacral and cervical spinal cord occurred in all three transgenic mouse lines with a severity that was highly dose-dependent. For TAR4/4 and TAR6/6 mice, although all spinal segments were affected, loss of the characteristic cervical and lumbosacral enlargements that innervate the extremities was remarkable. The number of neurons in the lumbosacral region in TAR4/4 mice was significantly lower than in Ntg littermates (608 ± 112 vs. 803 ± 125 per mm^2; $P < 0.001$) as was also observed in TAR6/6 mice (689 ± 107 vs. 768 ± 108 per mm^2; $P < 0.05$; Fig. 3*H* and Fig. S3). Further using ubiquitin immunohistochemistry, a dose-dependent accumulation of ubiquitinated proteins in spinal motor neurons was also observed for all lines, shown here for TAR4/4 mice (Fig. 3*A*). Employing phosphospecific TDP-43 antibodies that can recognize pathological TDP-43, we showed a punctate staining pattern of the nucleus and cytoplasm in ≈10%, ≈2%, and less than 1% of spinal neurons in TAR4/4, TAR6/6, and TAR4 mice, respectively. TAR4/4 mice also showed larger cytoplasmic aggregates as granulovacuolar bodies. More interestingly, NIIs of 2–2.5 μm in diameter were observed in ≈1% of spinal neurons in 22- to 24-day-old TAR4/4 mice, but not in 18-day-old or younger TAR4/4 or in other mouse lines (Fig. 3 *B–D*). The presence of NIIs was also accompanied by nuclear TDP-43 clearing. Transmission electron microscopy confirmed light microscopy data by showing presence of non-membrane-bound NIIs of 2–3 μm in diameter, composed of loosely packed granular material and 10- to 20-μm fibrils, and was also accompanied by neuritic changes (Fig. 3 *E* and *F*) as shown in ALS and FTLD patients (27, 28). Similar to GFAP staining in the motor cortex, neuronal inclusions were also marked by astrogliosis (Fig. 3*G*). In none of the mouse models at any disease stage did the NIIs or NCIs in brain or spinal cord stain for tau or α-synuclein, which are important exclusion criteria for TDP-43 proteinopathies.

Accumulation of Detergent-Soluble ≈25-kDa CTFs in Nuclear Fraction. Another characteristic feature of FTLD and ALS is accumulation of ≈25-kDa CTFs in affected brain and spinal cord regions (4, 5, 29). We thus characterized TDP-43 CTFs from brain of different TDP43^{WT} mice and different disease stages of TAR4/4 mice by immunoblotting with a panel of TDP-43 antibodies. Also, because TDP-43 has important nuclear functions, we analyzed the cytoplasmic and nuclear fractions separately. We first showed hTDP-43 full-length (FL) protein in both nuclear and cytoplasmic fractions; however, compared with Ntg mice, TAR4/4 mice showed increased levels of TDP-43 in the cytoplasmic fraction, whereas in the nuclear fraction, FL TDP-43 levels did not differ between TAR4/4 and Ntg mice (Fig. 4*A* and Fig. S6). These data suggest that levels of FL TDP-43 in the nucleus are tightly regulated. Similar observations were also made on TAR6/6 mice. Reprobing these blots revealed lamin A/C detection only in the nuclear fraction and GAPDH only in the cytoplasmic compartment, confirming a clear separation of nuclear and cytoplasmic fractions (Fig. 4*A Lower*). The ≈35-kDa CTFs were also recovered from both cytoplasmic and nuclear fractions from TDP43^{WT} mice but not from Ntg littermates. When analyzing different disease stages of TAR4/4 mice, the ≈35-kDa CTF levels decreased with increasing disease severity (Fig. 4*A* and Fig. S6). The identity of these fractions was also confirmed by immunoblotting with a C-t antibody (30) (Fig. 4*B*). Finally, the ≈25-kDa fragment was also specifically observed in TDP43^{WT} mice but only in the nuclear fraction, and increased with increasing disease severity in TAR4/4 mice ($P < 0.001$; Fig. 4*B*). These data suggest that ≈25-kDa TDP-43 fragments play a pathogenic role in these mouse models.

Because decreased solubility of TDP-43 or its cleaved fragments is also proposed as a disease mechanism (4, 5), we further determined the solubility of TDP-43 by sequential brain extraction with buffers of increasing detergent strengths (31). Though the majority of ≈35-kDa CTFs were recovered in low-salt (LS) fraction, and to some extent in Triton X-100 (Tx) fraction, FL TDP-43 was recovered from LS, Tx, sarkosyl-soluble (SARK), and, in a very small proportion, from the detergent-insoluble (urea) fraction. However, the ≈25-kDa CTFs were recovered solely in the Tx fraction that also solubilized nuclear lamin A/C protein (Fig. 4*C*). Interestingly, though presence of ≈25-kDa CTFs in the detergent-insoluble urea fraction is a hallmark feature of TDP-43 proteinopathy, these CTFs are also consistently recovered in the Tx-soluble nuclear fractions from

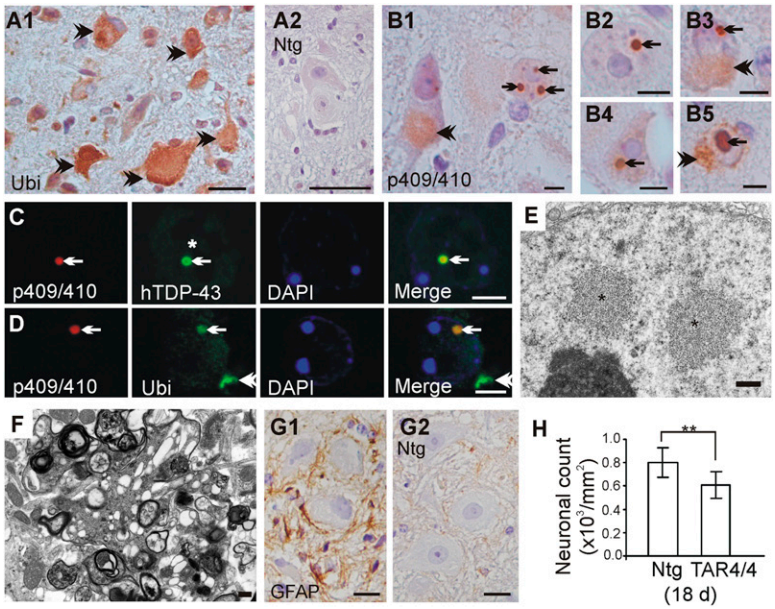

Fig. 3. Spinal cord NCI and NII pathology in TDP43^{WT} mice. (*A*) Ubiquitin pathology present in spinal motor neurons of TAR4/4 but absent in Ntg mice. (Scale bars: 20 μm.) (*B1–B4*) Lumbar spinal cord showing NIIs immunostained with phosphospecific p409/410 TDP-43 antibody that are remarkably similar to the round NIIs observed in FTLD-TDP patients (*B5*). *B1* shows frequently observed occurrence of more than one NII within a neuron (arrows) and of phospho-TDP-43-positive granulovacuoles in the cytoplasm (arrowhead). (Scale bars: 5 μm.) (*C* and *D*) Colabeling of p409/410 TDP-43 with human TDP-43 and ubiquitin antibodies. Arrow points to a NII, and asterisk in *C* denotes TDP-43 clearing in the NII-bearing neuron. Note the NCI in *D* (arrowhead) is negative for p409/410 TDP-43 reactivity. (Scale bars: 5 μm.) (*E* and *F*) Ultrastructural microscopy of lumbar spinal cord showing two non-membrane-bound, loosely packed NIIs (asterisks) in *E* and dystrophic neurites observed in the ventral exit zone in *F*. (Scale bars: 500 nm.) (*G*) GFAP immunohistochemistry showing increased astrogliosis that is absent in Ntg mice. (Scale bars: 10 μm.) (*H*) Quantification of the neurons showed ≈25% reduction in motor neurons in lumbosacral spinal cord of TAR4/4 mice compared with Ntg littermates (**$P < 0.01$).

brains of FTLD/ALS patients (Fig. 4*D* and Fig. S7). Because ≈25-kDa CTFs lack the predicted NLS sequence (6–9), we tested whether this hinders their transport to nucleus. Transiently transfecting two human cell lines (SH-SY5Y neuron-like cells and H4 neuroglioma cells) with a caspase-cleaved, GFP-tagged, TDP-43 CTF construct (TDP-43-Δ1–219-GFP) (32), we showed a predominant nuclear localization of this fragment (Fig. 4*E*). These data all indicate that ≈25-kDa CTFs can localize to the nucleus and progressively deposit in affected brain and spinal cord regions and associate with the phenotype we describe here, and is consistent with the idea that ≈25-kDa CTFs play a direct role in TDP-43-led neurodegeneration (4, 5, 29).

Discussion

Abnormal aggregation of proteins into fibrillar lesions is a neuropathological hallmark of several sporadic and hereditary neurodegenerative diseases, such as Alzheimer's disease, Parkinson disease, and Huntington disease (33). However, it is unclear whether it is the abnormal sequestration of protein in these aggregates or if they form the reservoir for the formation of low molecular weight oligomers as shown for a number of neurodegenerative diseases (33, 34). Identification of TDP-43 as a major ubiquitinated protein in FTLD-TDP and ALS patients has also led to a similar intense investigation into whether TDP-43 mediated neurodegeneration is through a gain of one or more toxic properties of the aggregates or a loss of normal TDP-43 function arising from sequestration of the normal protein in cellular aggregates (14, 29, 35, 36).

We report here a unique mouse model of TDP-43 developing large NCIs in vulnerable neurons characteristic of FTLD and ALS as well as NIIs characteristic of FTLD-TDP. The NIIs were almost always composed of ubiquitinated and phosphorylated TDP-43, and development of these inclusions coincided with the extremely rapid progression of disease in the TAR4/4 line. Thus, it remains possible that formation of NIIs contributed significantly to the disease progression. The NCIs in TDP43^{WT} mice also contained phosphorylated and ubiquitinated forms of TDP-43; however, in many such inclusions, TDP-43 was not the major ubiquitinated protein deposited. These data suggest that TDP-43 might trigger dysfunction of protein degradation pathways, such as the ubiquitin proteasome system and authophagy, which is a hallmark feature of neurodegenerative diseases (37).

Toxicity incurred by 22- to 25-kDa TDP-43 CTFs was proposed as a disease mechanism in sporadic ALS and FTLD patients (4, 5, 29). In support of these findings, we report here the generation and accumulation of ≈25-kDa TDP-43 CTFs in TDP43^{WT} mice that correlated with the disease progression in the TAR4/4 mouse line. Surprisingly, the ≈25-kDa CTFs were recovered from the nuclear compartment and not from the cytoplasm. Though the ≈25-kDa fragment importantly contains the conserved ribonucleoprotein RNP2 segment shown to bind to the TAR DNA sequence and RNA sequences with UG repeats involved in various TDP-43 functions, it lacks the nuclear localization signal (NLS) (6–9, 38). However, one of the shortest 25-kDa caspase-derived TDP-43 CTFs (TDP-43-Δ1–219) (32) despite lacking the NLS, predominantly localized to the nucleus when expressed in two human cell lines. X-ray crystallography data has shown that TDP-43 exists as a dimer, and the RRM2, of which the RNP2 is a part, is important in the β-strand and TDP-43 dimeric structure formation (39). Whether the ≈25-kDa CTFs are passively transported to the nucleus where it binds to endogenous TDP-43 or other targets, or is transported to nucleus in a dimeric state with full-length TDP-43, remains to be shown.

Recently, a mouse model of an ALS-associated mutant form of human TDP-43 driven by a mouse PrP promoter (PrP-TDP43^{A315T}) has been described where a 3-fold transgene overexpression leads to features of ALS and FTLD with average survival of ≈5 months (40). PrP-TDP43^{A315T} mice develop gait

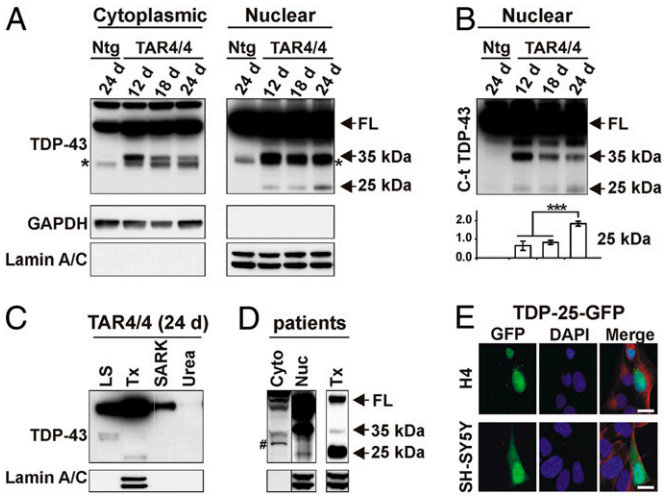

Fig. 4. TDP-43 processing in TDP43^{WT} mice. (*A*) Immunoblot of brain lysates of TAR4/4 mice with a non-species-specific TDP-43 antibody showing increased full-length (FL) TDP-43 in the cytoplasmic but not in the nuclear fraction compared with Ntg littermates (see short exposed blots and quantification in Fig. S6). Approximately 35-kDa CTFs are decreased with increasing disease severity in both nuclear and cytoplasmic fractions (Fig. S6), whereas the ≈25-kDa CTFs were only recovered from the nuclear fraction and correlated with disease progression. GAPDH was used as a marker for the cytoplasmic fraction and lamin A/C for the nuclear fraction. Asterisk at ≈34 kDa likely represents a known splice form of endogenous mouse TDP-43. (*B*) 35-kDa and 25-kDa bands stained with a C-terminal TDP-43 antibody showing the same trend of 35-kDa decrease and 25-kDa CTFs increase with increasing disease severity. The 25-kDa CTF band is quantified below (***$P <$ 0.001; error bars, SD). (*C*) Sequential extraction detected with a non-species-specific TDP-43 antibody showed the 35-kDa CTFs were mainly recovered from the LS fraction (and a small proportion in the Tx fraction), whereas the 25-kDa CTFs were recovered from the Tx fraction. LS, low salt; Tx, Triton X-100; SARK, sarkosyl. (*D*) Brain lysate of an FTLD-TDP patient showing that 25-kDa fragments are predominantly recovered from the nuclear fraction and in the Tx fraction in sequential extractions. #, non-disease-specific band. See also full sequential blot in Fig. S7. (*E*) Transfection of H4 and SH-SY5Y cells with 25-kDa TDP-43 CTF (Δ1–219) with a C-terminal GFP tag (TDP-25-GFP) showing that 25-kDa CTFs (green) predominantly localized in the nucleus (α-tubulin, red). (Scale bars: 10 μm.)

abnormalities and characteristic loss of vulnerable neurons, including cortical layer V pyramidal neurons in frontal cortex and spinal motor neurons, as also shown here for TDP43^{WT} mice. Although PrP-TDP43^{A315T} mice do not deposit TDP-43-positive NCIs or NIIs, characteristically observed for the highest-expressing TDP43^{WT} and probably related to transgene dose, interestingly, PrP-TDP43^{A315T} also accumulated ≈25-kDa CTFs in brain and spinal cord. Though Wegorzewska and co-workers (40) were unable to generate Prp-TDP-43 wild-type mice, we show here that ≈2.8-fold total TDP-43 neuronal expression in Thy-1 driven TDP43^{WT} mice is toxic to neurons, and ≈3.8-fold TDP-43 neuronal expression leads to mortality at ≈6 months. Though it is difficult to compare the relative toxicity of WT TDP-43 versus A315T mutant because PrP promoter drives expression in both neurons and glial cells, and the relative expression of endogenous TDP-43 in neurons and glial cells is unknown, it is clear that expression of TDP-43 is less well tolerated in mice compared with mutant SOD1 (mSOD1). For instance, at least two commonly used mSOD1 mouse lines have mutant protein accumulating to ≈10× levels over the already abundant endogenous SOD1 (22, 23). Also, TDP-43 dose is related to specific vulnerability of select neurons, as Thy-1 promoter driven expression is one of the highest in the dentate gyrus cells (24)—neurons that were not typically affected in the TDP-43^{WT} mice.

Finally, the fact that both overexpression of WT TDP-43 and an ALS mutant lead to similar disease in transgenic mice and an increase of ≈25-kDa TDP-43 fragments importantly suggests that *TARDBP* mutations identified in ALS patients likely act by a gain-of-function mechanism. Given the toxic effect of TDP-43 protein or its fragments, it is less likely that copy-number variations will be identified in ALS/FTLD patients; however, polymorphisms within the *TARDBP* 3′ UTR region have been identified that increase TDP-43 levels (41). Although a further genetic proof of TDP-43 dosage in ALS/FTLD is needed, interestingly, Wobbler mouse models of ALS due to mutation in the *Vps54* gene show up-regulation and accumulation of TDP-43 in brain (42, 43). Our data thus importantly suggest that targeting TDP-43 accumulates might be one therapeutic option in ALS-FTLD spectrum disorders involving TDP-43.

Note that while this paper was under review, a report on a TDP-43 knockout mouse model was published showing that heterozygous mice are phenotypically normal and without obvious motor-function defect (44).

Materials and Methods

Construction of Transgenic Mice Expressing Wild-Type Human TDP-43. *TARDBP* (NM_007375) was amplified from a human cDNA library (hTDP-43) and cloned into an mTUB expression vector containing a murine Thy-1 promoter (JSW Research). The expression vector was microinjected into pronuclear oocytes of Bl6/SJL mice by the Yale Transgenic Mouse Service Facility (New Haven, CT). Offspring were genotyped, and from 108 potential transgenic pups, 23 were identified to carry the transgene. Founders were bred with Ntg C57Bl6/J mice to establish stable transgenic lines. Additionally, homozygous hTDP-43-overexpressing mice were generated for two selected lines by crossbreeding hemizygous hTDP-43-overexpressing mice. Homozygosity was determined by semiquantitative PCR, and homozygous expression was confirmed by Q-RT-PCR and immunoblotting on brain tissue of 3-week-old mice. Although homozygous hTDP-43 mice were generated each time by crossbreeding of hemizygous mice, for sake of convenience, homozygous mice are also referred to as mouse lines. All animal experiments were approved by the University of Antwerp Ethics Committee and conducted according to the guidelines of the Federation of European Laboratory Animal Science Associations (FELASA).

Analysis of Integration Site. Thermal asymmetric interlaced (TAIL) PCR was performed to define the hTDP-43 chromosomal integration site essentially as described previously (45). Following TAIL-PCR, products were directly sequenced, and the specific chromosomal integration sites were identified using the UCSC BLAST database for *Mus musculus* genomic DNA (http://www.genome.ucsc.edu/, assembly: July 2007).

Tissue Preparation. Brains were harvested, weighed, and cut midsagittally. Left hemispheres were fixed in 2% paraformaldehyde (18-20 h) or 4% glutaraldehyde (4 h) and further prepared for histological or electron microscopy analysis, respectively. Right hemispheres were snap frozen in liquid nitrogen and stored at −80 °C for subsequent mRNA and protein analysis. Similarly, spinal cords subdivided into cervical, thoracic, lumbar, and sacrococcygeal regions were also processed as described for brain.

Immunoblotting. Cytoplasmic and nuclear fractions from brain were prepared as described earlier (46). Briefly, frozen tissue was weighed and homogenized in buffer containing 10 mM Hepes, 10 mM NaCl, 1 mM KH_2PO_4, 5 mM $NaHCO_3$, 5 mM EDTA, 1 mM $CaCl_2$, 0.5 mM $MgCl_2$ (10× vol/wt). After 10 min on ice, 2.5 M sucrose (0.5× vol/wt) was added. Next, tissue was homogenized and centrifuged at 6,300 × *g* for 10 min. The supernatant was collected as cytoplasmic fraction. The pellet was washed three times in TSE buffer (10 mM Tris, 300 mM sucrose, 1 mM EDTA, 0.1% Nonidet P-40, 10× vol/wt), homogenized, and centrifuged at 4,000 × *g* for 5 min. Finally the pellet was resuspended in RIPA with 2% SDS (5× vol/wt) as the nuclear fraction.

Also, proteins were sequentially extracted with buffers of increasing detergent strength (hypotonic, Triton X-100, myelin floatation, sarkosyl, and urea buffers) as described previously (31). All buffers were substituted with protease inhibitors (Complete Mixture; Roche) and phosphatase inhibitors (PhosphoStop; Roche) before use. The following antibodies were used: rabbit anti-TDP-43 (ProteinTech Group), human specific mouse anti-TDP-43 (against residues 205–222; Abnova), rabbit anti-C-terminal TDP-43 (C-t TDP-

43) (29), rabbit anti-TDP-43 phosphorylation sites 409/410 (TDP-43 p409/410) (21), rabbit anti-cleaved caspase-3, and rabbit anti-cleaved PARP (Cell Signaling Technology). Detection was performed using HRP-conjugated secondary antibodies and ECL Plus Chemiluminescent Detection System (Amersham Biosciences). Data were normalized to β-actin (Sigma), GAPDH (Meridian Life Science), or Lamin A/C (N-18; Santa Cruz Biotechnology).

Histology. Classical histochemistry was performed according to standard protocols (47). For immunohistochemistry, the following antibodies were used in addition to the ones mentioned for immunoblotting: mouse anti-ubiquitin (Zymed), rabbit anti-GFAP (Dako), and rabbit anti-Iba1 (Wako Chemicals). Antigen retrieval was performed with boiling in citrate buffer. All immunohistochemical analyses were performed on an Axioskop 50 light microscope (Zeiss) equipped with a CCD Olympus DP camera, an Axiovert 200M fluorescent microscope (Zeiss), or an LSM 700 confocal laser scanning microscope (Zeiss) as detailed elsewhere (27, 47).

Electron Microscopy. Brain and spinal cord were fixed in 4% buffered glutaraldehyde (4 h), transferred to glucose buffer, and finally to 2% buffered osmium tetraoxide before embedding and processing with standard protocols (27, 47). Grids were viewed and photographed on a Philips CM10 electron microscope.

ACKNOWLEDGMENTS. The authors thank Drs. Virginia M. Lee and Manuela Neumann for TDP-43 C-terminal antibodies, Dr. Masato Hasegawa for the phosphospecific TDP-43 p409/410 antibody, personnel of the VIB Genetic Service Facility (http://www.vibgeneticservicefacility.be/) for genetic analyses, and Martine Boogaerts for animal husbandry. This work was in part supported by the Medical Foundation Queen Elisabeth, the Foundation for Alzheimer Research (SAO/FRMA), the Interuniversity Attraction Poles (IAP) Program P6/43 of the Belgian Federal Science Policy Office, a Methusalem Excellence Grant from the Flemish Government, the Fund for Scientific Research–Flanders (FWO-V), the Institute for the Promotion of Innovation Through Science and Technology in Flanders (IWT-V), and the Special Research Fund of the University of Antwerp, Belgium. G.K. is holder of a PhD fellowship of the FWO-V and S.P. of the IWT-V.

1. Geser F, Martinez-Lage M, Kwong LK, Lee VM, Trojanowski JQ (2009) Amyotrophic lateral sclerosis, frontotemporal dementia and beyond: The TDP-43 diseases. *J Neurol*, 256:1205–1214 10.1007/s00415-009-5069-7.
2. Mackenzie IR, Feldman HH (2005) Ubiquitin immunohistochemistry suggests classic motor neuron disease, motor neuron disease with dementia, and frontotemporal dementia of the motor neuron disease type represent a clinicopathologic spectrum. *J Neuropathol Exp Neurol* 64:730–739.
3. Murphy JM, et al. (2007) Continuum of frontal lobe impairment in amyotrophic lateral sclerosis. *Arch Neurol* 64:530–534.
4. Neumann M, et al. (2006) Ubiquitinated TDP-43 in frontotemporal lobar degeneration and amyotrophic lateral sclerosis. *Science* 314:130–133.
5. Arai T, et al. (2006) TDP-43 is a component of ubiquitin-positive tau-negative inclusions in frontotemporal lobar degeneration and amyotrophic lateral sclerosis. *Biochem Biophys Res Commun* 351:602–611.
6. Buratti E, Baralle FE (2001) Characterization and functional implications of the RNA binding properties of nuclear factor TDP-43, a novel splicing regulator of CFTR exon 9. *J Biol Chem* 276:36337–36343.
7. Ayala YM, et al. (2005) Human, Drosophila, and C. elegans TDP43: Nucleic acid binding properties and splicing regulatory function. *J Mol Biol* 348:575–588.
8. Buratti E, et al. (2005) TDP-43 binds heterogeneous nuclear ribonucleoprotein A/B through its C-terminal tail: An important region for the inhibition of cystic fibrosis transmembrane conductance regulator exon 9 splicing. *J Biol Chem* 280:37572–37584.
9. Wang IF, Wu LS, Shen CK (2008) TDP-43: An emerging new player in neurodegenerative diseases. *Trends Mol Med* 14:479–485.
10. Sreedharan J, et al. (2008) TDP-43 mutations in familial and sporadic amyotrophic lateral sclerosis. *Science* 319:1668–1672.
11. Gitcho MA, et al. (2008) TDP-43 A315T mutation in familial motor neuron disease. *Ann Neurol* 63:535–538.
12. Benajiba L, et al.; French Clinical and Genetic Research Network on Frontotemporal Lobar Degeneration/Frontotemporal Lobar Degeneration with Motoneuron Disease (2009) TARDBP mutations in motoneuron disease with frontotemporal lobar degeneration. *Ann Neurol* 65:470–473.
13. Lagier-Tourenne C, Cleveland DW (2009) Rethinking ALS: The FUS about TDP-43. *Cell* 136:1001–1004.
14. Johnson BS, McCaffery JM, Lindquist S, Gitler AD (2008) A yeast TDP-43 proteinopathy model: Exploring the molecular determinants of TDP-43 aggregation and cellular toxicity. *Proc Natl Acad Sci USA* 105:6439–6444.
15. Tatom JB, et al. (2009) Mimicking aspects of frontotemporal lobar degeneration and Lou Gehrig's disease in rats via TDP-43 overexpression. *Mol Ther* 17:607–613.
16. Kollias G, et al. (1987) Differential regulation of a Thy-1 gene in transgenic mice. *Proc Natl Acad Sci USA* 84:1492–1496.
17. Brewer GJ, Torricelli JR (2007) Isolation and culture of adult neurons and neurospheres. *Nat Protoc* 2:1490–1498.
18. Kumar-Singh S, et al. (2006) Mean age-of-onset of familial alzheimer disease caused by presenilin mutations correlates with both increased Abeta42 and decreased Abeta40. *Hum Mutat* 27:686–695.
19. Duchen LW, Strich SJ, Falconer DS (1964) Clinical and pathological studies of an hereditary neuropathy in mice (dystonia musculorum). *Brain* 87:367–378.
20. Mackenzie IR, et al. (2009) Nomenclature for neuropathologic subtypes of frontotemporal lobar degeneration: Consensus recommendations. *Acta Neuropathol* 117:15–18.
21. Hasegawa M, et al. (2008) Phosphorylated TDP-43 in frontotemporal lobar degeneration and amyotrophic lateral sclerosis. *Ann Neurol* 64:60–70.
22. Gurney ME, et al. (1994) Motor neuron degeneration in mice that express a human Cu,Zn superoxide dismutase mutation. *Science* 264:1772–1775.
23. Wong PC, et al. (1995) An adverse property of a familial ALS-linked SOD1 mutation causes motor neuron disease characterized by vacuolar degeneration of mitochondria. *Neuron* 14:1105–1116.
24. Lein ES, et al. (2007) Genome-wide atlas of gene expression in the adult mouse brain. *Nature* 445:168–176.
25. Josephs KA, Dickson DW (2007) Hippocampal sclerosis in tau-negative frontotemporal lobar degeneration. *Neurobiol Aging* 28:1718–1722.
26. Geser F, et al. (2008) Evidence of multisystem disorder in whole-brain map of pathological TDP-43 in amyotrophic lateral sclerosis. *Arch Neurol* 65:636–641.
27. Pirici D, et al. (2006) Characterization of ubiquitinated intraneuronal inclusions in a novel Belgian frontotemporal lobar degeneration family. *J Neuropathol Exp Neurol* 65:289–301.
28. Lin WL, Dickson DW (2008) Ultrastructural localization of TDP-43 in filamentous neuronal inclusions in various neurodegenerative diseases. *Acta Neuropathol* 116: 205–213.
29. Igaz LM, et al. (2009) Expression of TDP-43 C-terminal fragments in vitro recapitulates pathological features of TDP-43 proteinopathies. *J Biol Chem* 284:8516–8524.
30. Igaz LM, et al. (2008) Enrichment of C-terminal fragments in TAR DNA-binding protein-43 cytoplasmic inclusions in brain but not in spinal cord of frontotemporal lobar degeneration and amyotrophic lateral sclerosis. *Am J Pathol* 173:182–194.
31. Sampathu DM, et al. (2006) Pathological heterogeneity of frontotemporal lobar degeneration with ubiquitin-positive inclusions delineated by ubiquitin immunohistochemistry and novel monoclonal antibodies. *Am J Pathol* 169:1343–1352.
32. Zhang YJ, et al. (2009) Aberrant cleavage of TDP-43 enhances aggregation and cellular toxicity. *Proc Natl Acad Sci USA* 106:7607–7612.
33. Hardy J, Selkoe DJ (2002) The amyloid hypothesis of Alzheimer's disease: Progress and problems on the road to therapeutics. *Science* 297:353–356.
34. Haass C, Selkoe DJ (2007) Soluble protein oligomers in neurodegeneration: Lessons from the Alzheimer's amyloid beta-peptide. *Nat Rev Mol Cell Biol* 8:101–112.
35. Ayala YM, Misteli T, Baralle FE (2008) TDP-43 regulates retinoblastoma protein phosphorylation through the repression of cyclin-dependent kinase 6 expression. *Proc Natl Acad Sci USA* 105:3785–3789.
36. Feiguin F, et al. (2009) Depletion of TDP-43 affects Drosophila motoneurons terminal synapsis and locomotive behavior. *FEBS Lett* 583:1586–1592.
37. Nedelsky NB, Todd PK, Taylor JP (2008) Autophagy and the ubiquitin-proteasome system: Collaborators in neuroprotection. *Biochim Biophys Acta* 1782:691–699.
38. Winton MJ, et al. (2008) Disturbance of nuclear and cytoplasmic TAR DNA-binding protein (TDP-43) induces disease-like redistribution, sequestration, and aggregate formation. *J Biol Chem* 283:13302–13309.
39. Kuo PH, Doudeva LG, Wang YT, Shen CK, Yuan HS (2009) Structural insights into TDP-43 in nucleic-acid binding and domain interactions. *Nucleic Acids Res* 37:1799–1808.
40. Wegorzewska I, Bell S, Cairns NJ, Miller TM, Baloh RH (2009) TDP-43 mutant transgenic mice develop features of ALS and frontotemporal lobar degeneration. *Proc Natl Acad Sci USA* 106:18809–18814.
41. Gitcho MA, et al. (2009) TARDBP 3′-UTR variant in autopsy-confirmed frontotemporal lobar degeneration with TDP-43 proteinopathy. *Acta Neuropathol* 118:633–645.
42. Shan X, Vocadlo D, Krieger C (2009) Mislocalization of TDP-43 in the G93A mutant SOD1 transgenic mouse model of ALS. *Neurosci Lett* 458:70–74.
43. Dennis JS, Citron BA (2009) Wobbler mice modeling motor neuron disease display elevated transactive response DNA binding protein. *Neuroscience* 158:745–750.
44. Wu LS, et al. (2009) TDP-43, a neuro-pathosignature factor, is essential for early mouse embryogenesis. *Genesis* 10.1002/dvg.20584.
45. Pillai MM, Venkataraman GM, Kosak S, Torok-Storb B (2008) Integration site analysis in transgenic mice by thermal asymmetric interlaced (TAIL)-PCR: Segregating multiple-integrant founder lines and determining zygosity. *Transgenic Res* 17: 749–754.
46. Guillemin I, Becker M, Ociepka K, Friauf E, Nothwang HG (2005) A subcellular prefractionation protocol for minute amounts of mammalian cell cultures and tissue. *Proteomics* 5:35–45.
47. Kumar-Singh S, et al. (2005) Dense-core plaques in Tg2576 and PSAPP mouse models of Alzheimer's disease are centered on vessel walls. *Am J Pathol* 167:527–543.